nature electronics

Article

https://doi.org/10.1038/s41928-023-01069-w

Brain organoid reservoir computing for artificial intelligence

Received: 1 March 2023

Accepted: 13 October 2023

Published online: 11 December 2023

Check for updates

Hongwei Cai[1], Zheng Ao[1], Chunhui Tian[1], Zhuhao Wu[1], Hongcheng Liu[2], Jason Tchieu[3,4], Mingxia Gu[3,4], Ken Mackie[5] & Feng Guo[1]

Brain-inspired computing hardware aims to emulate the structure and working principles of the brain and could be used to address current limitations in artificial intelligence technologies. However, brain-inspired silicon chips are still limited in their ability to fully mimic brain function as most examples are built on digital electronic principles. Here we report an artificial intelligence hardware approach that uses adaptive reservoir computation of biological neural networks in a brain organoid. In this approach—which is termed Brainoware—computation is performed by sending and receiving information from the brain organoid using a high-density multielectrode array. By applying spatiotemporal electrical stimulation, nonlinear dynamics and fading memory properties are achieved, as well as unsupervised learning from training data by reshaping the organoid functional connectivity. We illustrate the practical potential of this technique by using it for speech recognition and nonlinear equation prediction in a reservoir computing framework.

The recent success of artificial intelligence (AI) has been largely driven by the development of artificial neural networks (ANNs)[1], which process large datasets using silicon computing chips[2,3]. However, training ANNs on current AI computing hardware is energy intensive and time consuming[4,5]. The physical separation of data from data-processing units—known as the von Neumann bottleneck[6,7]—is a key cause of these issues. The slowing of Moore's law also places further limitations on current AI hardware[8,9]. Thus, alternative approaches for the development of AI hardware are needed[9,10].

The human brain is a complex three-dimensional biological network of about 200 billion cells, which are linked to one another via hundreds of trillions of nanometre-sized synapses[11,12]. Its structure, function and efficiency could be a powerful source of inspiration for the development of AI hardware. In particular, a human brain typically expends about 20 watts, whereas current AI hardware consumes about 8 million watts to drive a comparative ANN[5]. The brain can also effectively process and learn information from noisy data at minimal training cost through neuronal plasticity and neurogenesis[13,14], avoiding the large energy consumption of high-precision computing approaches[11,12].

The human brain fuses data storage and processes within biological neural networks (BNNs)[15,16], naturally avoiding any von Neumann bottleneck issues. Inspired by BNNs, attempts have been made to develop high-efficiency and low-cost neuromorphic chips—using memristors, for example[10,17–20]—that store previously experienced current or/and voltages in internal states and enable short-term memory[21–23]. Such neuromorphic chips have been used for various applications, for example, in computer vision[24,25] and speech recognition[26,27]. However, current neuromorphic chips can only partially mimic brain functions, and there is a need to improve their processing capability and accounting for real-life uncertainty and improving energy efficiency.

Brain organoids are in vitro three-dimensional aggregates that are created through the self-organization and differentiation of human pluripotent stem cells and can become brain-like tissues that can recapitulate aspects of a developing brain's structure and function[28–31].

[1]Department of Intelligent Systems Engineering, Indiana University Bloomington, Bloomington, IN, USA. [2]Department of Industrial and Systems Engineering, University of Florida, Gainesville, FL, USA. [3]Center for Stem Cell & Organoid Medicine (CuSTOM), Division of Pulmonary Biology, Division of Developmental Biology, Cincinnati Children's Hospital Medical Center, Cincinnati, OH, USA. [4]University of Cincinnati School of Medicine, Cincinnati, OH, USA. [5]Gill Center for Biomolecular Science, Department of Psychological and Brain Sciences, Indiana University Bloomington, Bloomington, IN, USA. e-mail: fengguo@iu.edu

https://doi.org/10.1038/s41928-023-01069-w

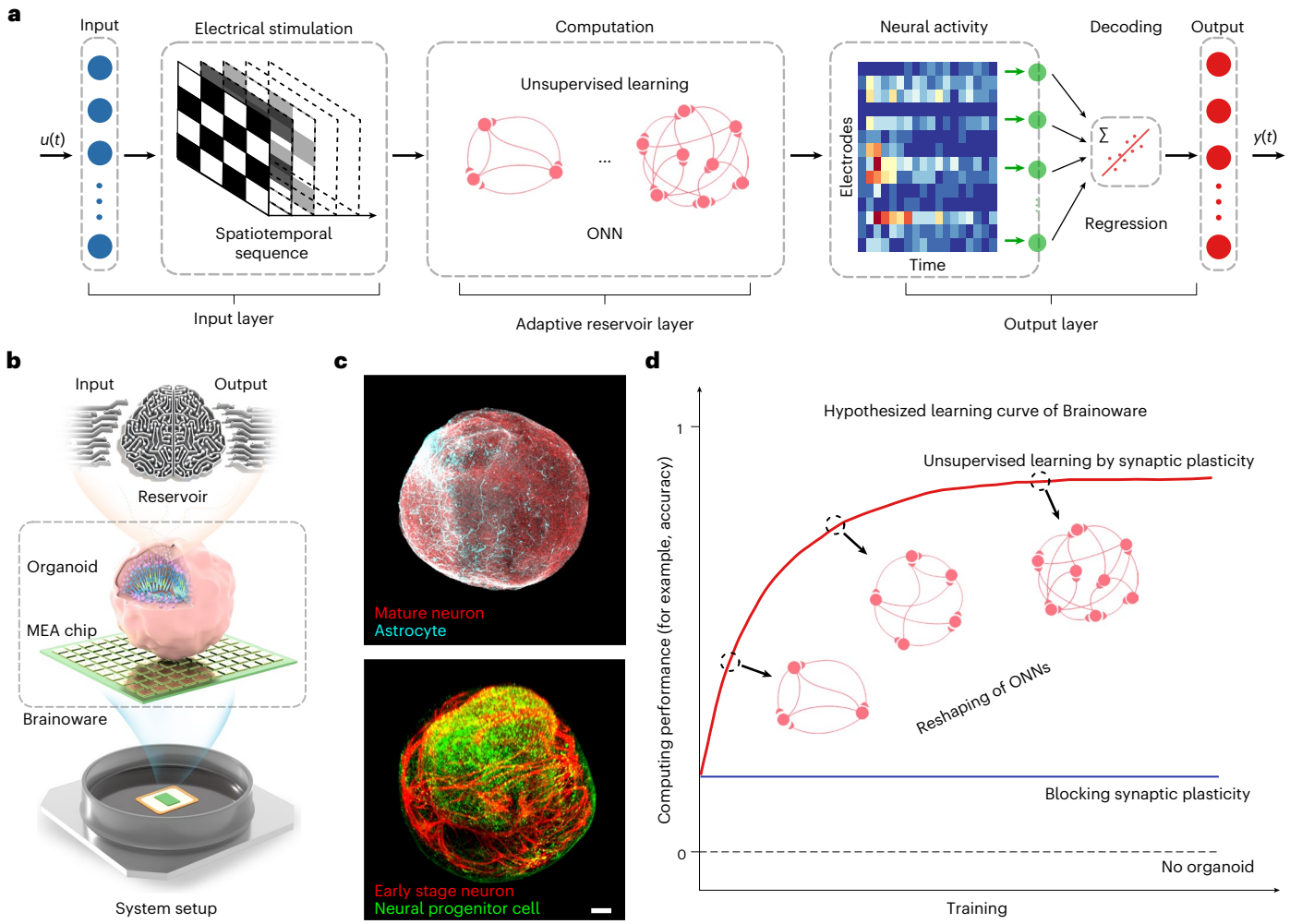

Fig. 1 | Brainoware with unsupervised learning for AI computing. a, Schematic of an adaptive reservoir computing framework using Brainoware. **b**, Schematic of the paradigm of Brainoware setup that mounts a single brain organoid onto a high-density MEA for receiving inputs and sending outputs. **c**, Whole-mount immunostaining of cortical organoids showing complex three-dimensional neuronal networks with various brain cell identities (for example, mature neuron, MAP2; astrocyte GFAP; neurons of early differentiation stage, TuJ1; neural progenitor cells, SOX2). **d**, Schematic demonstrating the hypothesized, unsupervised learning of Brainoware by reshaping the BNN during training, and the inhibition of unsupervised learning after synaptic plasticity is blocked. Scale bar, 100 μm.

In this Article, we report an AI hardware that harnesses the reservoir computation and unsupervised learning ability of organoid neural networks (ONNs) in a brain organoid. The approach—termed Brainoware—processes spatiotemporal information, and achieves unsupervised learning, probably through the neuroplasticity of the brain organoid (Fig. 1a and Supplementary Fig. 1). Compared with current two-dimensional (2D) in vitro neuronal cultures and neuromorphic chips (Supplementary Table 1), Brainoware could provide additional insights for AI computing because brain organoids can provide BNNs with complexity, connectivity, neuroplasticity and neurogenesis, as well as low energy consumption and fast learning.

Brainoware with unsupervised learning for AI computing

We constructed Brainoware by mounting a functional brain organoid onto a high-density multielectrode array (MEA) (Fig. 1b). The human brain organoid for Brainoware was characterized by various brain cell identities (for example, early stage and mature neurons, astrocytes and neuron progenitor cells), and early development of brain-like structures (for example, ventricular zones and subventricular zones) for the formation, function and maintenance of complex ONNs (Fig. 1c and Supplementary Fig. 2), as well as network electrical activity (Supplementary Fig. 3 and Supplementary Video 1). The ONNs received inputs via external electrical stimulation and sent outputs via evoked neural activity, offering a functional basis for AI computing. As a proof-of-concept application, we implemented Brainoware as a reservoir computing framework[32]. In conventional reservoir computing hardware, the input signals can be mapped into higher-dimensional computational spaces through a reservoir, which is a 'black box' comprising the dynamics of a physical system. Given specific input signals, the output of this reservoir is used as features for a simple 'readout function' (for example, a linear or logistic regression model) to perform a computational task, for example, classification and time-series analysis. Although conventional reservoir dynamics are fixed, the readout function is trained to map the feature values generated by the reservoir to the desired labels of the data. Different from conventional reservoir computing hardware with a fixed physical reservoir, Brainoware uses a human brain organoid as 'an adaptive living reservoir' to conduct 'unsupervised learning'. The time-dependent inputs can be converted into spatiotemporal sequences of electric stimulation through an input layer, and then projected into high-dimensional computational spaces as ONNs via the adaptive living reservoir. The output signals, as neural

https://doi.org/10.1038/s41928-023-01069-w

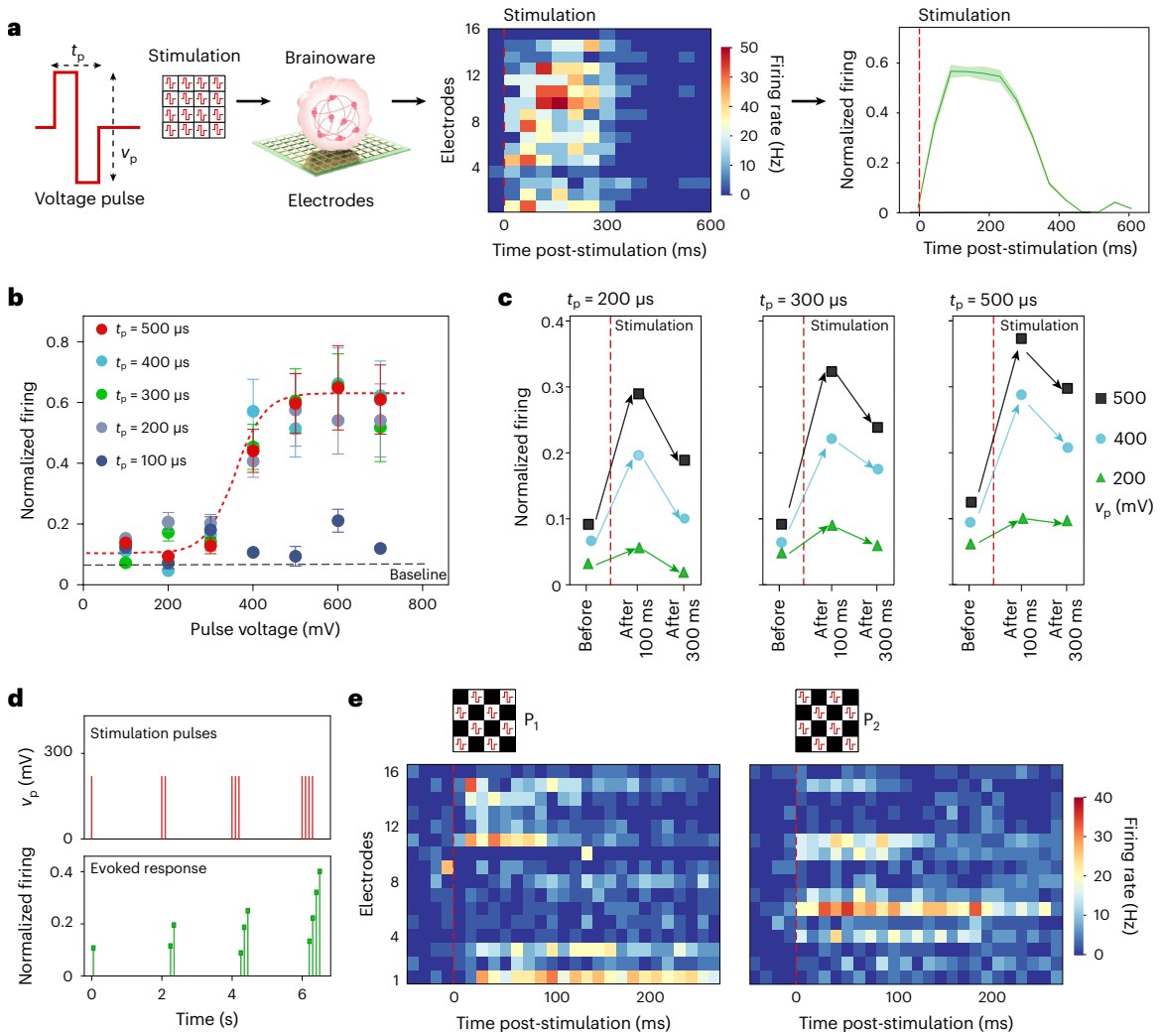

Fig. 2 | Reservoir computing hardware properties. a, Evoked response (raster plot and post-stimulation histogram) on a single bipolar voltage pulse stimulation (mean ± standard error of the mean (s.e.m.), $n = 5$ stimulation trials). **b**, Representative evoked normalized firing on pulses with different pulse times (t_p) and pulse voltages (v_p) (mean ± standard deviation, $n = 5$ stimulation trials; Supplementary Fig. 5). The red fitting curve (a sigmoid function) indicates nonlinear activity, whereas the black dashed line marks spontaneous activity. **c**, Representative evoked normalized firing before, after 100 ms or after 300 ms from the end of single-pulse stimulation (Supplementary Fig. 6), showing the fading dynamics. **d**, Representative memristor-like responses to a stream of pulses ($v_p = 200$ mV, $t_p = 300$ µs). **e**, Distinct raster plots evoked by two complementary spatial patterns (namely, P1 and P2) of stimulation pulses ($v_p = 500$ mV, $t_p = 500$ µs).

activities, can be effectively utilized via a readout function for various tasks (Fig. 1a and Supplementary Fig. 1). Moreover, by training using the spatiotemporal sequences of electrical stimulation, Brainoware can improve its computing performance and demonstrate unsupervised learning via the adaptive living reservoir. This is possible because Brainoware responds to the electric stimulations with changes in the functional connectivity of the organoids[33,34] (Supplementary Fig. 4 and Supplementary Video 2), enabling the dynamic reshaping of ONNs. If the synaptic plasticity is blocked (for example, by K252A—a blocker for activity-dependent synaptic plasticity), the computing performance is maintained by Brainoware (but unsupervised learning of the adaptive reservoir halts) (Figs. 1d and 4d). In the following experiments, Brainoware was demonstrated to exhibit unique and critical properties of a physical reservoir and we successfully conduct some real-world tasks with limited training data at low energy and computing cost.

Reservoir computing hardware properties

Before applying Brainoware to reservoir computing tasks, we characterized and demonstrated its basic implementation as a physical reservoir. We tested the physical reservoir properties of Brainoware such as nonlinear dynamics, fading memory (or short-term memory) and spatial information processing by checking the response of ONNs to bipolar voltage pulse stimulations with different pulse times (t_p) and voltages (v_p). For example, as electrical stimulation pulses are applied to Brainoware, the evoked neuronal activity (raster plot) was recorded, and the post-stimulation histogram was calculated and plotted (Fig. 2a). We demonstrated that Brainoware exhibited a representative nonlinear response to the pulse voltage (Fig. 2b and Supplementary Fig. 5). After applying a single voltage pulse stimulation ($t_p \geq 200$ µs), the evoked mean normalized firing rate of Brainoware (over 200 ms post-stimulation) to the pulse voltage can be fitted with a sigmoid function, in accordance with the nonlinear activation function of ANNs. Although applying a single voltage pulse stimulation with short pulse times ($t_p < 200$ µs), the evoked normalized firing of Brainoware with the same organoid was only around the baseline of its spontaneous activity. Next, we tested the fading memory of Brainoware by applying pulses with different pulse times and voltages. The evoked normalized firing of Brainoware before and after 100 or 300 ms from the end of

https://doi.org/10.1038/s41928-023-01069-w

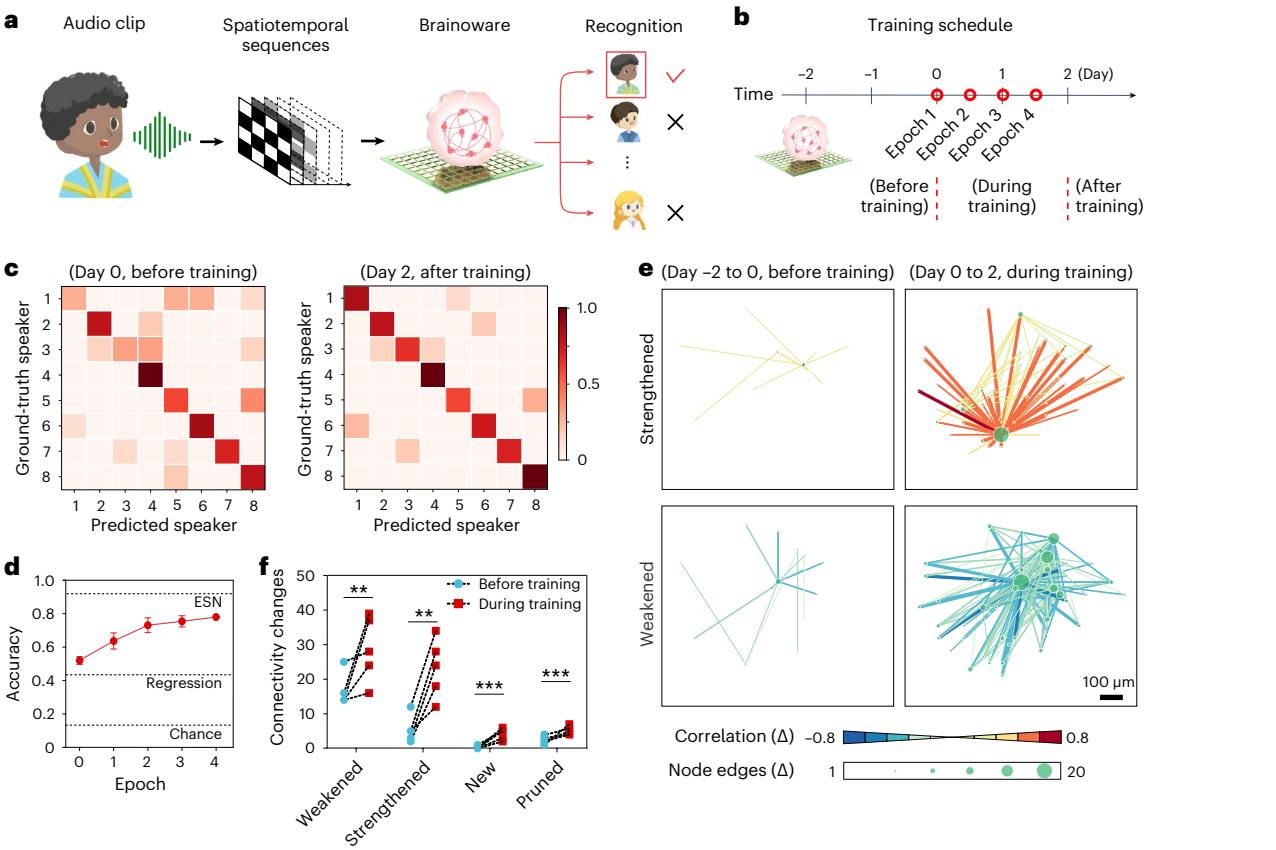

Fig. 3 | Speech recognition. a, Workflow of performing a speech recognition task using Brainoware. **b**, Schematic showing that Brainoware with the naïve organoid receives daily training from day 0 to 2 with one epoch (whole Japanese vowel dataset) per half-day. **c**, Representative confusion matrix showing the speech recognition performance before and after training. **d**, Increase in speech recognition accuracy over training epochs (mean ± s.e.m., $n = 5$ organoids, from three independent experiments). The three dashed lines represent the accuracy by chance (Chance), accuracy by a logistic regression algorithm (Regression) and accuracy by a standard reservoir computing algorithm called echo state network (ESN). **e**, Functional connectivity changes in the same organoid from days −2 to 0 (before training) and from days 0 to 2 (during training), indicating the unsupervised learning of Brainoware from training. **f**, Quantification of connectivity changes (weakened, strengthened, new and pruned) before and during training (mean ± s.e.m., $n = 5$ organoids, from three independent experiments; unpaired t-test, $^{**}P = 0.0083$, $^{**}P = 0.0029$, $^{***}P = 0.0008$, $^{***}P = 0.0012$; Supplementary Fig. 9).

single-pulse stimulation was obtained (Fig. 2c and Supplementary Fig. 6). Pulses with longer duration and higher voltage were responsible for stronger evoked response and slower relaxation dynamics. Importantly, the nonlinear response and fading dynamics of ONNs can be well controlled by precisely adjusting the stimulation parameters (Supplementary Fig. 7a). Moreover, we also demonstrated the combination of these two properties within Brainoware. After the application of four individual trains of pulses ($v_p = 200$ mV, $t_p = 300$ μs), Brainoware showed both accumulation and decay of dynamic responses (Fig. 2d and Supplementary Fig. 7b). Multiple pulses at short intervals (50 ms) within a pulse train were responsible for the gradual increase in evoked responses and the delay of relaxation dynamics, in accordance with the dynamic response of a memristor—a typical reservoir computing hardware. Furthermore, we demonstrated the capability of Brainoware to process spatial information. The spatial information was converted into spatial patterns of simulation pulses ($v_p = 500$ mV, $t_p = 500$ μs) such as two 4 × 4 spatial patterns (namely, P1 and P2). The distinct raster plots of Brainoware with the same organoid were evoked by these two complementary patterns and showed the active storage and gradual loss of different spatial information over time (Fig. 2e), indicating spatial information processing rather than stimulation artifacts.

Speech recognition

To apply Brainoware for performing real-world time-series tasks, we demonstrated speech recognition by distinguishing an individual speaker's vowels from a speaker pool (Fig. 3a). A benchmark test of speech recognition was implemented using a Japanese vowel database. Here 240 audio clips of isolated Japanese vowels (/a/ and /e/) pronounced by eight different male speakers (as one epoch) were converted into spatiotemporal sequences of stimulation bipolar pulses and applied to Brainoware. The evoked ONN activity (for example, raster plot) was recorded and fed into a logistic regression function for classification. After training the logistic regression algorithm and optimizing the stimulation (Supplementary Fig. 8), Brainoware could be applied to speech recognition. Brainoware, starting with a naïve organoid, received training from days 0 to 2 with one epoch every 12 h (Fig. 3b). Before training, a representative confusion matrix was experimentally obtained (Fig. 3c, left), but only a low accuracy was reached at about 51.0 ± 7.8%. These results indicate that Brainoware may employ the pre-existing functional connectivity of the naïve organoid to perform the speech recognition task (Supplementary Fig. 9). After training Brainoware with the same organoid for four training epochs, another representative confusion matrix was experimentally obtained (Fig. 3c, right), and higher accuracy was achieved, at about 78.0 ± 5.2%, highlighting that Brainoware improved its performance of speech recognition by training. Moreover, Brainoware increased its accuracy of speech recognition over training epochs (Fig. 3d). These results indicate that the electrical stimulation during training may trigger the unsupervised learning of Brainoware for improving computing performance by reshaping the functional connectivity of the organoid.

https://doi.org/10.1038/s41928-023-01069-w

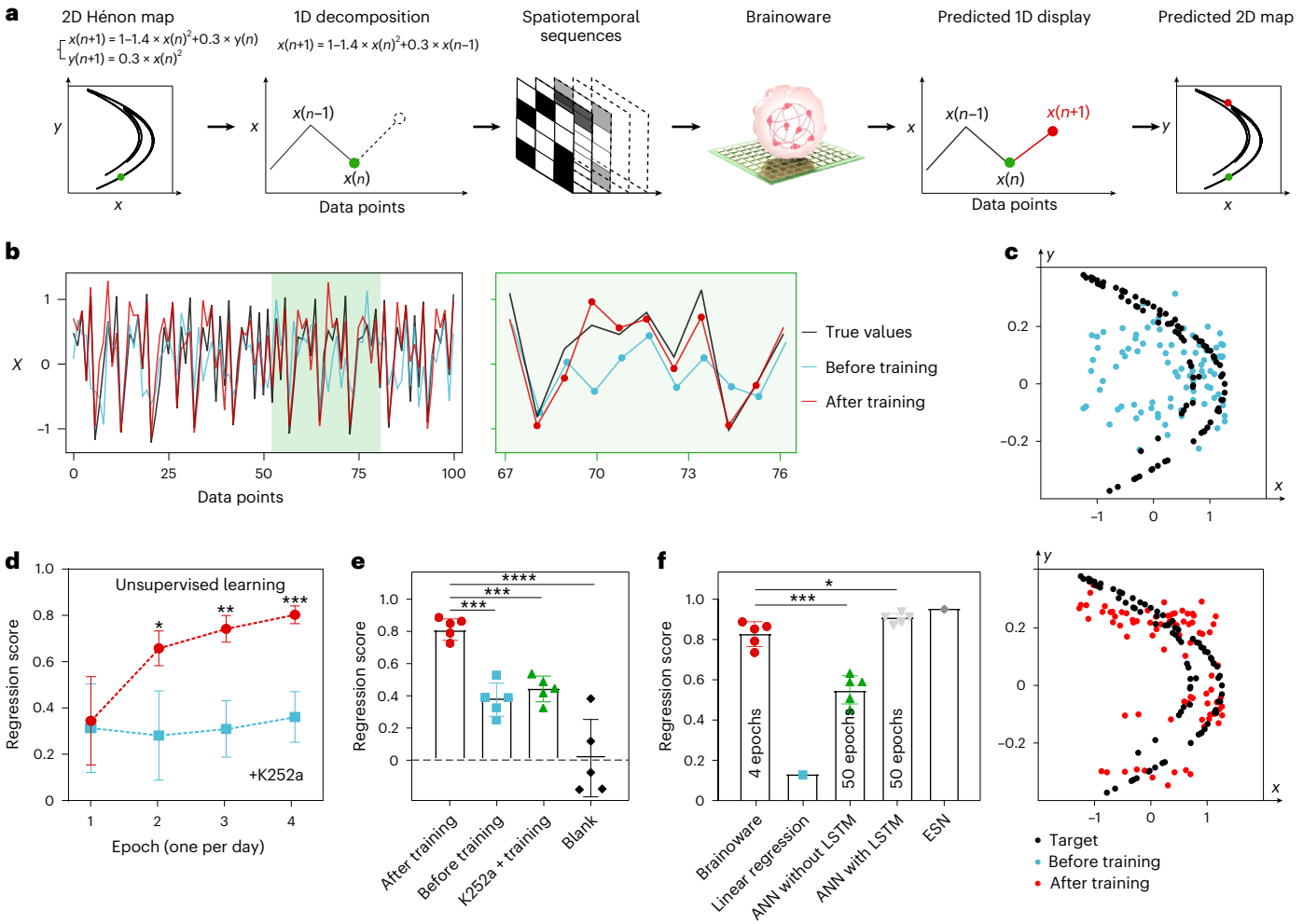

Fig. 4 | Predicting a nonlinear chaotic equation. a, Workflow of predicting a Hénon map. **b**, Predicted *X* values using Brainoware before (blue) and after training (red) versus ground true *X* value (black). **c**, Predicted 2D maps using Brainoware before (blue) and after (red) training versus ground true 2D map (black). **d**, Learning curves of Brainoware over training epochs, where the red or blue curves show Brainoware with naïve organoids or organoids treated with a CaMKII blocker K252a (to block synaptic plasticity) before training (mean ± s.e.m., $n = 5$ organoids, from three independent experiments; $^{*}P = 0.0259$, $^{**}P = 0.007$, $^{***}P = 0.0004$). **e**, Learning activity of Brainoware under different conditions with the naïve organoids (before training), organoids after training (after training), organoids treated with K252a during training (K252a + training) and without organoids (blank) (mean ± s.e.m., $n = 5$ organoids, from three independent experiments; $^{***}P = 0.001$, $^{***}P = 0.0004$, $^{****}P < 0.0001$). **f**, Performance comparison of Brainoware with linear regression, ANN with or without an LSTM unit and a standard reservoir computing algorithm (ESN). The number denotes the training epochs of each group (mean ± s.e.m., $n = 5$ organoids, from three independent experiments; Supplementary Fig. 11; $^{*}P = 0.013$, $^{***}P = 0.0087$).

To test this, the functional connectivity changes in a naïve organoid before training (days −2 to 0) and the same organoid during training (days 0 to 2) were separately measured (Fig. 3e and Supplementary Fig. 9). More tests also demonstrated that the trained organoids (during training) have significantly more connectivity changes (for example, weakened, strengthened, new and pruned conditions) than the naïve organoids (before training) (Fig. 3f). These results indicate that training notably reshapes the functional connectivity of the organoid, possibly facilitating the unsupervised learning ability of Brainoware.

Predicting a nonlinear chaotic equation

We further applied Brainoware to predict a Hénon map, which is a typical nonlinear dynamic system with chaotic behaviour. This time-series task was implemented into Brainoware using a brief workflow (Fig. 4a). A 2D Hénon map was first converted into a one-dimensional (1D) decomposition, converted into the spatiotemporal sequences of bipolar voltage pulses, optimized using the delay- and place-encoding methods and then sent to the MEA electrodes for stimulating Brainoware (Supplementary Fig. 10). Using a simple readout linear regression algorithm for decoding the neural activity of the organoid (Supplementary Fig. 10), Brainoware harnessed its adaptive reservoir computation to achieve unsupervised learning from the input spatiotemporal pulses and predict the Hénon map. Experiments were conducted to predict the Hénon map (X_{n+1} value) by feeding Brainoware with spatiotemporal pulses encoded with X_n value. The 1D decomposition (Fig. 4b) and 2D displacement (Fig. 4c) of the predicted Hénon maps were experimentally obtained from Brainoware with the same organoid before and after four training epochs (one epoch per day, and each epoch encoded with a Hénon map dataset of 200 data points). Here, compared with the theoretical output (ground truth; black), the after-training condition (red) showed better-predicted results than the before-training condition (blue). Next, the learning curves of Brainoware to predict this nonlinear chaotic equation were measured over epochs (Fig. 4d). The accuracy of Brainoware in predicting the X_{n+1} value was used to evaluate its learning ability to predict the Hénon map. Interestingly, Brainoware increased the regression score (Supplementary Information provides the detailed calculation) from 0.356 ± 0.071 (with the naïve organoids) to 0.812 ± 0.043 (the same

organoids after four training epochs). Although treated with a calcium/calmodulin-dependent protein kinase II (CaMKII) blocker, namely, K252a, to block activity-dependent synaptic plasticity[35], the negative control group only slightly improved their regression score from 0.310 ± 0.072 to 0.385 ± 0.063 over the same training procedures. The results indicated that the learning activity of Brainoware was dependent on neural plasticity. Furthermore, experiments were performed to measure the unsupervised learning activities of Brainoware under different conditions (Fig. 4e). Only an MEA chip and culture medium (blank) were tested to have a regression score of 0, emphasizing that Brainoware cannot compute without the organoids. We further compared Brainoware with representative machine learning algorithms such as ANN on predicting the Hénon map of the same data size (Fig. 4f). Linear regression (decoding algorithm of Brainoware) could barely predict this problem, showing an accuracy close to 0. Brainoware notebly outperformed ANN without a long short-term memory (LSTM) unit (Supplementary Fig. 11). Brainoware (with 4 training epochs) showed slightly lower accuracy than ANN with LSTM (each with 50 training epochs), decreasing the training times by >90%.

Conclusions

We have reported a class of reservoir computing hardware that harnesses the computational power of ONNs. Human brain organoids have the ability to self-organize and form functional ONNs for the development of brain-inspired AI hardware. The ONNs may also have the necessary complexity and diversity to mimic a human brain, which could inspire the development of more sophisticated and human-like AI systems[36,37]. Due to the high plasticity and adaptability of organoids, Brainoware has the flexibility to change and reorganize in response to electrical stimulation, highlighting its ability for adaptive reservoir computing. The approach may also naturally address the challenges regarding time and energy consumption and heat production of current AI hardware. We showed that our approach can exhibit physical reservoir properties such as nonlinear dynamics, fading memory and spatial information processing. We also implemented it in practical applications: speech recognition and nonlinear equation prediction. Furthermore, we showed that the approach can learn from training data by reshaping the functional connectivity of ONNs.

There are several limitations and challenges with the current Brainoware approach. One technical challenge is the generation and maintenance of organoids. Despite the successful establishment of various protocols, current organoids still suffer from high heterogeneity, low generation throughput, necrosis/hypoxia and various viabilities. Moreover, it is critical to properly maintain and support organoids to harvest their computational power. Recent engineering efforts focused on optimizing organoid differentiation and growth conditions, and manipulating their microenvironments may provide approaches for the high-throughput generation and maintenance of standardized organoids[38].

The power consumption of the current Brainoware hardware is low, but the additional peripheral equipment required (such as CO_2 incubator and computer) still consume considerable power. In the future, and based on electronics developments and system integration, it should be possible to integrate customized systems for maintaining and interfacing of organoids with very low power consumption. Brainoware uses flat and rigid MEA electrodes for interfacing with organoids, which are only able to stimulate/record a small number of neurons on the organoid surface. Thus, there is a need to develop methods—such as brain–machine interfaces and soft electrodes[39–41]—to interface the whole organoid with AI hardware and software[42,43]. This should allow the exchange of information, as well as the manipulation of their activity, from a greater number of neurons. Another technical challenge is the management and analysis of data. The encoding and decoding of temporospatial information to and from Brainoware still needs to be optimized through improvements in data interpretation, extraction and processing from multiple sources and modalities[44–46]. Moreover, large amounts of data may be generated by this new AI hardware, which could require the development of new algorithms and methods for analysing and visualizing the data.

Methods

Generation and characterization of organoids

Cortical organoids were generated from human pluripotent stem cells following a protocol that we adapted from the reported protocols[28,47]. All the handling and culture of stem cells and organoids followed the guidelines of the WiCell Institute and Indiana University Biosafety Committee. Supplementary Information and Methods provide detailed protocols for the development and characterization of organoids.

System setups

The hardware used to assemble the system included a humidified incubator (Heracell VIOS 160i, Thermo Fisher) maintained at 37 °C and 5% CO_2 for culturing and maintaining the organoid, a MaxOne MEA system (Maxwell) for interfacing the organoid and a personal computer to run Python (3.6.13) and Maxlive (22.2.4 software by the MEA manufacturer) for implementing the reservoir computing frame of Brainoware. Supplementary Information and Methods provide detailed information on plating, stimulating and recording organoids.

Software

The software used to assemble the system included Maxlive for generating the stimulation sequence, giving stimulation and recording the evoked neuronal activity, and Python for extracting and processing of spikes, as well as feeding the processed signals into a readout function. Supplementary Information and Methods provide details about the computing framework.

Reservoir computing framework

Brainoware was implanted in a reservoir computing framework with three key components: an input layer, a reservoir layer and an output layer. The input layer converted information (image pattern, audio clips, time series and so on) into various spatiotemporal sequences of electrical stimulation pulses to the organoid (reservoir layer). The organoid (reservoir layer) received the input electrical stimulation ($u(t)$) and mapped to a high-dimensional computational space as the ONN. The neural activities representing the reservoir state were recorded by an MEA system and fed into a decoding function (for example, linear regression or logistic regression) to output $y(t)$, as an output layer for classification, recognition, prediction and other applications. Supplementary Information and Methods provide detailed information on the encoding, decoding and implementing of applications (for example, audio recognition and Henón map equation).

Statistical analysis

The statistics comparing two sample groups were conducted using the Students' t-test. Statistical significance was denoted as follows: $^{*}P < 0.05$, $^{**}P < 0.01$, $^{***}P < 0.005$, $^{****}P < 0.001$. Due to the exploratory nature of our experiments, we did not use statistical methods to predetermine the sample sizes, but our sample sizes are similar to previous reports[28,33,34] in the field of brain organoids.

Reporting summary

Further information on research design is available in the Nature Portfolio Reporting Summary linked to this article.

Data availability

Source data are provided with this paper. All other data that support the findings of this study are available from the corresponding author upon reasonable request.

References

1. Tang, J. et al. Bridging biological and artificial neural networks with emerging neuromorphic devices: fundamentals, progress, and challenges. *Adv. Mater.* **31**, e1902761 (2019).
2. Sejnowski, T. J. & Rosenberg, C. R. Parallel networks that learn to pronounce English text. *Complex Syst.* **1**, 145–168 (1987).
3. Samarasinghe, S. *Neural Networks for Applied Sciences and Engineering: From Fundamentals to Complex Pattern Recognition* (Auerbach Publications, 2016).
4. Gokmen, T. & Vlasov, Y. Acceleration of deep neural network training with resistive cross-point devices: design considerations. *Front. Neurosci.* **10**, 333 (2016).
5. Mehonic, A. & Kenyon, A. J. Brain-inspired computing needs a master plan. *Nature* **604**, 255–260 (2022).
6. Xia, Q. & Yang, J. J. Memristive crossbar arrays for brain-inspired computing. *Nat. Mater.* **18**, 309–323 (2019).
7. Wang, Z. R. et al. Resistive switching materials for information processing. *Nat. Rev. Mater.* **5**, 173–195 (2020).
8. Tanaka, G. et al. Recent advances in physical reservoir computing: a review. *Neural Netw.* **115**, 100–123 (2019).
9. Zidan, M. A., Strachan, J. P. & Lu, W. D. The future of electronics based on memristive systems. *Nat. Electron.* **1**, 22–29 (2018).
10. Grollier, J. et al. Neuromorphic spintronics. *Nat. Electron.* **3**, 360–370 (2020).
11. Marković, D., Mizrahi, A., Querlioz, D. & Grollier, J. Physics for neuromorphic computing. *Nat. Rev. Phys.* **2**, 499–510 (2020).
12. Goswami, S. et al. Decision trees within a molecular memristor. *Nature* **597**, 51–56 (2021).
13. Purves, D. et al. *Neurosciences* (De Boeck Supérieur, 2019).
14. Parisi, G. I., Kemker, R., Part, J. L., Kanan, C. & Wermter, S. Continual lifelong learning with neural networks: a review. *Neural Netw.* **113**, 54–71 (2019).
15. Krogh, A. What are artificial neural networks? *Nat. Biotechnol.* **26**, 195–197 (2008).
16. Schmidhuber, J. Deep learning in neural networks: an overview. *Neural Netw.* **61**, 85–117 (2015).
17. Milano, G. et al. *In materia* reservoir computing with a fully memristive architecture based on self-organizing nanowire networks. *Nat. Mater.* **21**, 195–202 (2022).
18. Sillin, H. O. et al. A theoretical and experimental study of neuromorphic atomic switch networks for reservoir computing. *Nanotechnology* **24**, 384004 (2013).
19. Strukov, D. B., Snider, G. S., Stewart, D. R. & Williams, R. S. The missing memristor found. *Nature* **453**, 80–83 (2008).
20. Torrejon, J. et al. Neuromorphic computing with nanoscale spintronic oscillators. *Nature* **547**, 428–431 (2017).
21. Zhang, W. Q. et al. Neuro-inspired computing chips. *Nat. Electron.* **3**, 371–382 (2020).
22. Wang, Z. et al. Memristors with diffusive dynamics as synaptic emulators for neuromorphic computing. *Nat. Mater.* **16**, 101–108 (2017).
23. Yang, J. J., Strukov, D. B. & Stewart, D. R. Memristive devices for computing. *Nat. Nanotechnol.* **8**, 13–24 (2013).
24. Yao, P. et al. Face classification using electronic synapses. *Nat. Commun.* **8**, 15199 (2017).
25. Li, C. et al. Analogue signal and image processing with large memristor crossbars. *Nat. Electron.* **1**, 52–59 (2018).
26. Moon, J. et al. Temporal data classification and forecasting using a memristor-based reservoir computing system. *Nat. Electron.* **2**, 480–487 (2019).
27. Zhong, Y. et al. Dynamic memristor-based reservoir computing for high-efficiency temporal signal processing. *Nat. Commun.* **12**, 408 (2021).
28. Trujillo, C. A. et al. Complex oscillatory waves emerging from cortical organoids model early human brain network development. *Cell Stem Cell* **25**, 558–569 (2019).
29. Lancaster, M. A. et al. Cerebral organoids model human brain development and microcephaly. *Nature* **501**, 373–379 (2013).
30. Chiaradia, I. & Lancaster, M. A. Brain organoids for the study of human neurobiology at the interface of in vitro and in vivo. *Nat. Neurosci.* **23**, 1496–1508 (2020).
31. Qian, X. et al. Brain-region-specific organoids using mini-bioreactors for modeling ZIKV exposure. *Cell* **165**, 1238–1254 (2016).
32. Lukoševičius, M. & Jaeger, H. Reservoir computing approaches to recurrent neural network training. *Comput. Sci. Rev.* **3**, 127–149 (2009).
33. Giandomenico, S. L. et al. Cerebral organoids at the air-liquid interface generate diverse nerve tracts with functional output. *Nat. Neurosci.* **22**, 669–679 (2019).
34. Sharf, T. et al. Functional neuronal circuitry and oscillatory dynamics in human brain organoids. *Nat. Commun.* **13**, 4403 (2022).
35. Canossa, M. et al. Neurotrophin release by neurotrophins: implications for activity-dependent neuronal plasticity. *Proc. Natl Acad. Sci. USA* **94**, 13279–13286 (1997).
36. Smirnova, L. et al. Organoid intelligence (OI): the new frontier in biocomputing and intelligence-in-a-dish. *Front. Sci.* **1**, 1017235 (2023).
37. Magliaro, C. & Ahluwalia, A. To brain or not to brain organoids. *Front. Sci.* **1**, 1148873 (2023).
38. Hofer, M. & Lutolf, M. P. Engineering organoids. *Nat. Rev. Mater.* **6**, 402–420 (2021).
39. Huang, Q. et al. Shell microelectrode arrays (MEAs) for brain organoids. *Sci. Adv.* **8**, eabq5031 (2022).
40. Park, Y. et al. Three-dimensional, multifunctional neural interfaces for cortical spheroids and engineered assembloids. *Sci. Adv.* **7**, eabf9153 (2021).
41. Li, T. L. et al. Stretchable mesh microelectronics for the biointegration and stimulation of human neural organoids. *Biomaterials* **290**, 121825 (2022).
42. Weltman, A., Yoo, J. & Meng, E. Flexible, penetrating brain probes enabled by advances in polymer microfabrication. *Micromachines* **7**, 180 (2016).
43. Lin, S. et al. A flexible, robust, and gel-free electroencephalogram electrode for noninvasive brain-computer interfaces. *Nano Lett.* **19**, 6853–6861 (2019).
44. Kagan, B. J. et al. In vitro neurons learn and exhibit sentience when embodied in a simulated game-world. *Neuron* **110**, 3952–3969.e3958 (2022).
45. Bakkum, D. J., Chao, Z. C. & Potter, S. M. Spatio-temporal electrical stimuli shape behavior of an embodied cortical network in a goal-directed learning task. *J. Neural Eng.* **5**, 310 (2008).
46. Chao, Z. C., Bakkum, D. J. & Potter, S. M. Shaping embodied neural networks for adaptive goal-directed behavior. *PLoS Comput. Biol.* **4**, e1000042 (2008).
47. Ao, Z. et al. Understanding immune-driven brain aging by human brain organoid microphysiological analysis platform. *Adv. Sci.* **9**, e2200475 (2022).

Acknowledgements

F.G. wants to acknowledge support from the National Institute of Health Awards (DP2AI160242, R01DK133864 and U01DA056242). We also acknowledge Indiana University Imaging Center (NIH1S10OD024988-01).

Author contributions

F.G. and H.C. conceived the study and designed the experiments. H.C., Z.A., C.T. and Z.W. performed the experiment. H.C., H.L., J.T., M.G. and K.M. analysed the data. F.G. and H.C. wrote the paper. All authors read and provided feedback on the paper.

Competing interests
The authors declare no competing interests.

Additional information
Supplementary information The online version contains supplementary material available at https://doi.org/10.1038/s41928-023-01069-w.

Correspondence and requests for materials should be addressed to Feng Guo.

Peer review information *Nature Electronics* thanks Arti Ahluwalia and the other, anonymous, reviewer(s) for their contribution to the peer review of this work.

nature portfolio

Corresponding author(s): Feng Guo

Last updated by author(s): Nov 10, 2023

Reporting Summary

Nature Portfolio wishes to improve the reproducibility of the work that we publish. This form provides structure for consistency and transparency in reporting. For further information on Nature Portfolio policies, see our Editorial Policies and the Editorial Policy Checklist.

Statistics

For all statistical analyses, confirm that the following items are present in the figure legend, table legend, main text, or Methods section.

n/a	Confirmed	
☐	☒	The exact sample size (*n*) for each experimental group/condition, given as a discrete number and unit of measurement
☐	☒	A statement on whether measurements were taken from distinct samples or whether the same sample was measured repeatedly
☐	☒	The statistical test(s) used AND whether they are one- or two-sided *Only common tests should be described solely by name; describe more complex techniques in the Methods section.*
☒	☐	A description of all covariates tested
☒	☐	A description of any assumptions or corrections, such as tests of normality and adjustment for multiple comparisons
☐	☒	A full description of the statistical parameters including central tendency (e.g. means) or other basic estimates (e.g. regression coefficient) AND variation (e.g. standard deviation) or associated estimates of uncertainty (e.g. confidence intervals)
☐	☒	For null hypothesis testing, the test statistic (e.g. *F*, *t*, *r*) with confidence intervals, effect sizes, degrees of freedom and *P* value noted *Give P values as exact values whenever suitable.*
☒	☐	For Bayesian analysis, information on the choice of priors and Markov chain Monte Carlo settings
☒	☐	For hierarchical and complex designs, identification of the appropriate level for tests and full reporting of outcomes
☒	☐	Estimates of effect sizes (e.g. Cohen's *d*, Pearson's *r*), indicating how they were calculated

Our web collection on statistics for biologists contains articles on many of the points above.

Software and code

Policy information about availability of computer code

Data collection	MaxLab Live (Maxwell Biosystem 22.2.4) to stimulate and record electrical activity from organoids.
Data analysis	Graphpad Prism (8.0.64) for bar graph plots and t-test analysis between groups. Kilosort (2.0) dependent on Matlab (R2020b) for spike sorting and single unit activity identification. Decoding and network analysis was performed using Python (3.6.13) Scikit-learn (0.24.2) for decoding functions including linear regression and logistic regression Elephant (0.10.0) for analyzing functional connectivity (spike_time_tiling_coefficient) Networkx (2.5.1) for functional connectivity plots

For manuscripts utilizing custom algorithms or software that are central to the research but not yet described in published literature, software must be made available to editors and reviewers. We strongly encourage code deposition in a community repository (e.g. GitHub). See the Nature Portfolio guidelines for submitting code & software for further information.

Data

Policy information about availability of data

All manuscripts must include a data availability statement. This statement should provide the following information, where applicable:

- Accession codes, unique identifiers, or web links for publicly available datasets
- A description of any restrictions on data availability
- For clinical datasets or third party data, please ensure that the statement adheres to our policy

All data are available in the main text or the supplementary figures.

Human research participants

Policy information about studies involving human research participants and Sex and Gender in Research.

Reporting on sex and gender	N/A
Population characteristics	N/A
Recruitment	N/A
Ethics oversight	N/A

Note that full information on the approval of the study protocol must also be provided in the manuscript.

Field-specific reporting

Please select the one below that is the best fit for your research. If you are not sure, read the appropriate sections before making your selection.

☒ Life sciences ☐ Behavioural & social sciences ☐ Ecological, evolutionary & environmental sciences

For a reference copy of the document with all sections, see nature.com/documents/nr-reporting-summary-flat.pdf

Life sciences study design

All studies must disclose on these points even when the disclosure is negative.

Sample size	For each experiments, we included 5-6 individual human cortical organoids in each group. Due to the exploratory nature of our experiments, we did not use statistical methods to pre-determine sample sizes, but our sample sizes are similar to the previous reports in brain organoids field.
Data exclusions	Bad samples (organoid without sufficient neuronal activity) were excluded prior to data collection, so no data samples needed exclusion.
Replication	All quantifications were done on three independent organoid batches, with a minimum of 5 cortical organoids per group.
Randomization	The cortical organoids of same batch were randomly selected and grouped for experiments.
Blinding	N/A

Reporting for specific materials, systems and methods

We require information from authors about some types of materials, experimental systems and methods used in many studies. Here, indicate whether each material, system or method listed is relevant to your study. If you are not sure if a list item applies to your research, read the appropriate section before selecting a response.

Materials & experimental systems

n/a	Involved in the study
☐	☒ Antibodies
☐	☒ Eukaryotic cell lines
☒	☐ Palaeontology and archaeology
☒	☐ Animals and other organisms
☒	☐ Clinical data
☒	☐ Dual use research of concern

Methods

n/a	Involved in the study
☒	☐ ChIP-seq
☒	☐ Flow cytometry
☒	☐ MRI-based neuroimaging

Antibodies

Antibodies used

CTIP2 Abcam AB18465
TBR2 Millipore AB15894
SOX2 R&D AF2018-SP
PAX6 BioLegend 901301
GFAP Abcam ab7260
MAP2 Millipore AB5543
PSD-95 Cell Signaling 3450S
HOPX Sigma HPA030180
Tuj1 Cell Signaling D71G9

Validation

These antibodies are validated by manufacturers for immunofluorescence, and these antibodies are also used and reported in the previous literatures.

Eukaryotic cell lines

Policy information about cell lines and Sex and Gender in Research

Cell line source(s)	WiCell - WA09
Authentication	WA09 cell line was authenticated by WiCell for research use.
Mycoplasma contamination	The cell line was not tested fro mycoplasma contamination.
Commonly misidentified lines (See ICLAC register)	No commonly misidentified cell lines were used.